

## Electromagnetic Levitation – White-noise Measurement Protocol for Modulated Calorimetry

Jacqueline ETAY

### Abstract

Electromagnetic levitation of electrically conductive droplets by alternating magnetic fields is a technique used to measure the physical properties of liquid metallic alloys as heat capacity and thermal diffusivity, among others. In order to reduce electromagnetic stirring and shaping of the molten sample, experiments are conducted in microgravity<sup>1)</sup>. Measurement is performed by using the modulation calorimetry technique [2][3]. Here we test both numerically and experimentally a new measurement protocol, which aim is to eliminate calibration. We use this procedure to demonstrate that the use of a levitator in a DC magnetic field overcomes the negative effects of the electromagnetic stirring inside the sample on the accuracy of the modulated calorimetry technique.

**Keyword(s):** Electromagnetic levitation, modulated calorimetry, identification, white-noise, magnetic fields superposition

### 1. Introduction

Numerical models of casting and solidification are increasingly used to optimize industrial processes for the production of metal alloys. All such models require, as input parameters, reliable thermophysical property values such as heat capacity and thermal conductivity. However, most standard measurement techniques, such as differential scanning calorimetry, require a molten metallic sample to be in contact with a crucible, leading to unavoidable contamination of this sample. Based on the early work of Okress<sup>4)</sup> on electromagnetic (e.m.) levitation, Egry, see for example<sup>5)</sup>, developed an electromagnetic levitator (EML), a non-contact technique, which when used in microgravity conditions, reduces flows inside the molten sample. This instrument is used in the framework of the Thermolab ESA-MAP project (Fecht<sup>6)</sup>).

In this article, we first present how the experimental device works. Then we briefly sum up the modulation calorimetry technique where thermal behavior of levitated sample is deduced from unsteady thermal simulation.

In the present work, signals are processed by a signal analysis technique coming from Process Engineering (Schetelat<sup>7)</sup>). It couples both a white-noised modulated input power and an identification procedure. This procedure allows to derivate relevant transfer functions of the considered system. The eigenfrequencies of those functions are relevant from external and internal heat exchanges of the sample.

First, calculated time-dependant temperatures are used as experimental recorded signals. This sequence is performed numerically both on solid and liquid, both varying viscosity and intensity of a superposed DC transverse magnetic field. Electromagnetic stirring effects on heat transfer are deduced

from the comparison between solid and liquid results. Analysis of the obtained results gives clear insights on how to manage modulated calorimetry to find reliable value of both heat capacity and thermal conductivity.

Second, we present experimental tests performed on a solid niobium bar. Experimental and literature results are compared.

### 2. Measuring principle

The principle of the measure is given by Fecht<sup>2)</sup> and by Wunderlich<sup>3)</sup>. It is sketched on **Fig.1**.

A spherical sample of radius  $R$  and electrical conductivity  $\sigma$  is located in an inductor powered by a high frequency alternating current:  $I_o \cos \omega_1 t$ ,  $I_o$  and  $\omega$  being the peak current and the angular frequency respectively. This inductor generates a magnetic field which induces, inside the sample, electrical inside the inductor and system representation of the arrangement (inductor+sample) currents localized in a surface layer called the electromagnetic skin depth. The effects

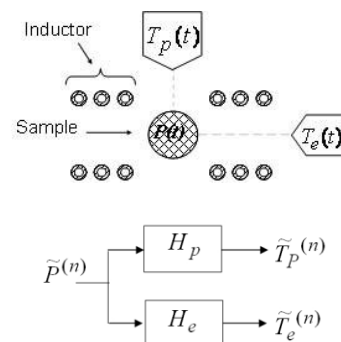


**Fig. 1** Schematic representation of the sample.

of these currents are twofold. First, they generate a Joule heating power  $P$  inside the sample. Second, they compose with the magnetic field to create a body force field able to center (or levitate) the sample.

When the sample is liquid, those body forces generate electromagnetic stirring. In the molten sample, the resulting velocity field evolves as the Alfvén velocity - given by the balance between inertia and electromagnetic forces term in the momentum equation -  $U_A \propto (I_o/R)\sqrt{\mu/\rho}$ , where  $\rho$  and  $\mu$  are the density of the sample and the permittivity of the vacuum respectively. A Reynolds number, defined as,  $R_A = U_A R/\nu$  where  $\nu$  is the kinematic viscosity, will be used to characterize the electromagnetic stirring.

Moreover, as proposed by Bojarevics<sup>8)</sup> to damp electromagnetic stirring motion, a transverse uniform continuous magnetic field  $B_{DC}$  can be applied. The non-dimensional number characterizing the effect of this DC field is the Hartman number  $Ha = B_{DC} R \sqrt{\sigma/\rho\nu}$ . Note that, such a tool is not yet set up on a real levitation device.

Modulated calorimetry consists in perturbing the thermal equilibrium of the sample by modulating the total Joule power  $P$  around its mean value  $\bar{P}$  ( $P = \bar{P} + \tilde{P}$ ) and recording the related time-dependent behavior of surface temperatures, i.e.  $T_p(t) = \bar{T}_p + \tilde{T}_p(t)$  and  $T_e(t) = \bar{T}_e + \tilde{T}_e(t)$  the polar and the equatorial temperatures. Currently, an analytical model<sup>2)</sup> is used and writes as :

$$C_p g_e \frac{d\tilde{T}_e}{dt} = h_{int} [\tilde{T}_p - (1 + s_e Bi) \tilde{T}_e] + \tilde{P} \quad (1)$$

$$C_p (1 - g_e) \frac{d\tilde{T}_p}{dt} = h_{int} [\tilde{T}_e - (1 + (1 - s_e) Bi) \tilde{T}_p] \quad (2)$$

where  $s_e$ ,  $g_e$ ,  $h_{int}$ , and  $Bi$  are respectively the surface area and the volume ratios of the equatorial zone, the internal global heat transfer coefficient and the Biot number.

It is established that for a well-tuned  $\omega_2$  modulation frequency of the Joule input power,  $\tilde{P} = P_o \cos(\omega_2 t)$ ,  $C_p$  and  $\kappa_{th}$  respectively the heat capacity and the thermal conductivity can be calculated by using the following equations

$$C_p = \frac{P_o}{\omega_2 \tilde{T}_p} \frac{1}{[1 + (g_e(1 - s_e) + s_e(1 - g_e)) Bi]} \quad (3)$$

$$\kappa_{th} = \frac{C_p g_e (1 - g_e) \omega_2^2}{4\pi(R - \gamma\delta)\omega_{ext}} \quad (4)$$

where  $\gamma$  and  $\delta$  are respectively a geometrical factor and the electromagnetic skin depth.

To use this model, calibrations are needed to establish the values of  $s_e$  and  $g_e$  the geometrical factors and  $\omega_{ext}$  the characteristic angular frequency of the heat transfer from the sample to its environment.

The measuring system is sketched on **Fig. 1**-top when on the bottom a system representation of the responses to the modulated power is presented. The functions  $H_p$  and  $H_e$  are the transfer functions relative to the pole and equatorial

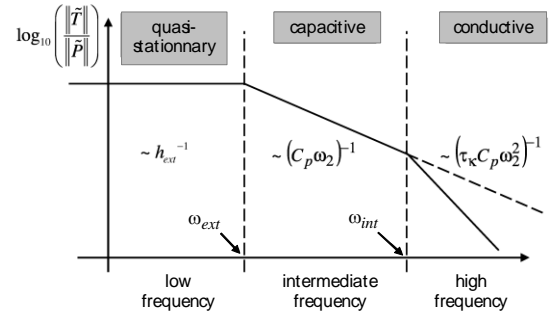


**Fig. 2** Characteristic thermal behavior in a solid sample versus the modulation frequency value.

temperature behaviors respectively.

To illuminate how the sample should reacts to different modulation frequencies  $\omega_2$ , we draw, on **Fig. 2**, a schematic thermal behavior of the sample versus  $\omega_2$ . It is defined as the ratio of the amplitude of the temperature fluctuation  $\tilde{T}_p$  on the amplitude of the power fluctuation  $\tilde{P}$ . For low frequency values  $\omega_2$ , the heat exchange between the sample and the exterior is dominating, leading to an almost stationary regime. Therefore the time variation of the sample temperature follows the time variation of the dissipated Joule power leading to a flat spectrum. For very high frequencies, that is to say greater than a critical value  $\omega_{int}$ , temporal variations of the temperature variations do not follow power variations anymore, the slope of the spectrum changes. When the sample is solid, it is a conductive regime and the slope is found to be equal to  $\omega_{int}/C_p\omega_2^2$ . For intermediate values, both internal and external heat exchanges control the temperature field. This is the range to choose the modulation frequency of the input power, when it is harmonic, i.e. depending on one frequency only<sup>3)</sup>. As proposed by Schetelat<sup>7)</sup>, using a white-noised input power, allows the experimenter to investigate the complete thermal behavior of the sample, giving him dispense to the knowledge of the geometry of this sample and to the choice of a specific modulation angular frequency.

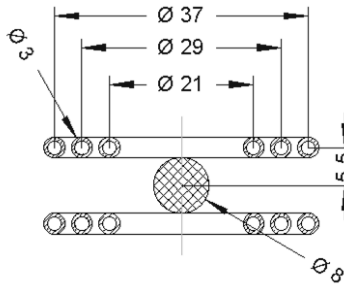
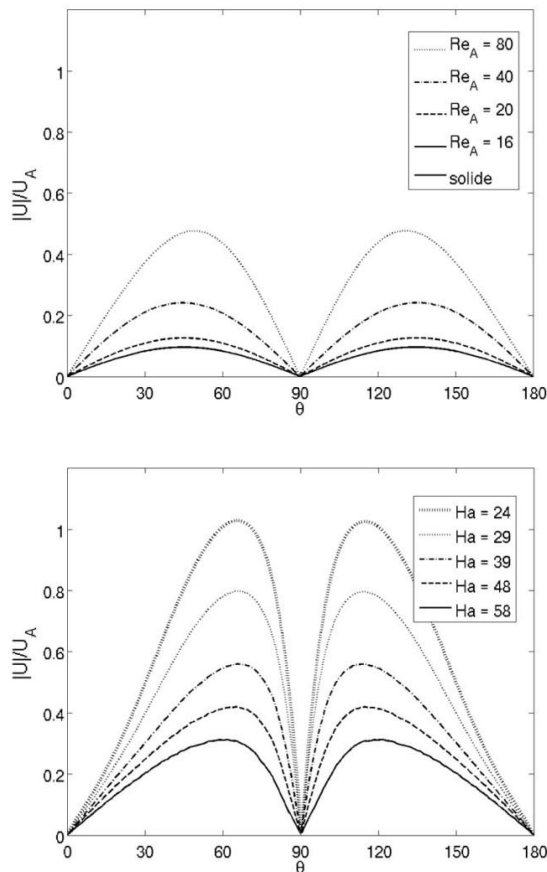
Such spectrum allows us to find  $\omega_{ext}$  and  $\omega_{int}$  two natural, also called eigen-frequencies calculated as the frequencies at which the slope of the spectrum changes.  $\omega_{ext}$  is inverse of the characteristic time of heat transfer between the sample and the surrounding atmosphere, when  $\omega_{int}$  is related to the time of transfer inside the sample. Therefore, the  $\omega_{int}$  value will possibly be affected by the flow. We will show that this value can be use to find  $C_p$  and  $\kappa_{th}$  attached to a solid sample or to a liquid sample when the EML is located in a DC magnetic field.

### 3. Simulation – Geometry and Software

To test the procedure outlined in the introduction section, we choose the geometry of **Fig. 3** and the simulation parameters given in **Table 1**. These geometry and parameters are chosen

**Table 1** Simulations parameters

sample radius $R$ , mm	4
density $\rho$ , $\text{kg.m}^{-3}$	3860
heat capacity $C_p$ , $\text{J.K}^{-1}.\text{kg}^{-1}$	663
thermal conductivity $\kappa_{th}$ , $\text{W.m}^{-1}.\text{K}^{-1}$	23.1
electrical conductivity $\sigma_{el}$ , $\Omega^{-1}.\text{m}^{-1}$	$5.26 \cdot 10^5$
total hemispherical emissivity $\varepsilon$	0.4
inductor current $I_0$ , $A_{\text{peak}}$	65
currents angular frequency $\omega_1$ , $\text{rad.s}^{-1}$	$2\pi \cdot 350 \cdot 10^3$


**Fig. 3** Sample and inductor geometries

**Fig. 4** Calculated velocity on the surface of a spherical sample varying  $Re_A$  (top) and  $Ha$  (bottom).

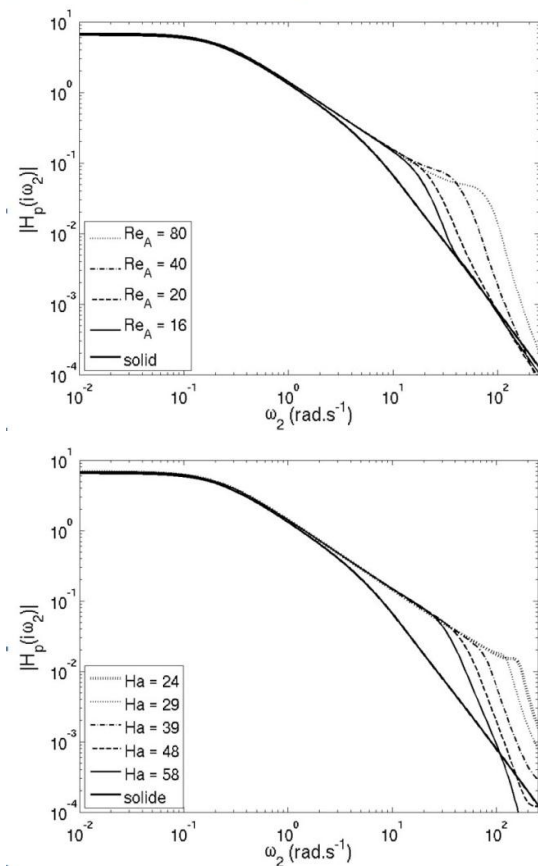
because they are representative of the on-board EML in parabolic flights, sounding rockets and the International Space Station. All physical properties are kept constant, i.e. not depending on temperature.

To emulate the temperature signals, we use the Fluent software in which Delannoy<sup>9)</sup> added a modulus that describes induction.

For those calculations, the Alfvén velocity is fixed to  $U_A = 0.3733 \text{ m.s}^{-1}$ . We choose conditions such that the flows remind laminar. Indeed, we know that the presence of turbulence would prevent measurements. We will go back to this assumption in the concluding section. The upper DC magnetic field intensity is limited to 1.2 Teslas by the used mesh.

Surface velocities, normalized by the Alfvén velocity and calculated under various viscosity conditions are plotted on **Fig. 4**. On the top, the Reynolds number  $Re_A$  varies, when, on the bottom, the intensity of the DC applied magnetic field varies, the liquid viscosity being fixed at  $\nu_0 = 10^{-6} \text{ m}^2.\text{s}^{-1}$ .

As expected, calculated flows are symmetrical about the equator ( $\theta = 90^\circ$ ). Those shapes are corresponding to two vortices in the bulk flow. The turnover angular frequency of the


**Fig. 5** Polar transfer function calculated by procedure proposed in<sup>8)</sup> and corresponding to motions presented on **Fig. 4**- top : varying viscosity – bottom : varying intensity of the DC magnetic field applied transversally.

bulk flow is calculated as  $\omega_{vortex} = \langle \nabla \times U \rangle / 2$ . Comparing both the left and right graphs, we see they are quite similar. Nevertheless, the point where the surface velocity is maximum is closer to the equator ( $\theta = 90^\circ$ ) in the presence of an applied DC magnetic field than in its absence. In such a case, this point range is  $\theta = 45^\circ$  and  $135^\circ$  (for  $Re_A = 16$ ) and  $\theta = 50^\circ$  and  $130^\circ$  (for  $Re_A = 80$ ).

How the flow changes the temperature field has been reported by Schetelat<sup>10</sup>. His conclusions were that, on the one hand, convection homogenizes the temperature field in the sample bulk and on the other hand, when active enough, it causes a temperature inversion near the equator. This generates a paradoxical phenomenon: in the equatorial zone where the input Joule power density is maximal and the temperature the lowest.

Once we have emulated the power and the corresponding velocity field, we use a pseudo white noise signal to modulate the power. It is generated by a Linear Feed Back Shift Register, commonly used in electronics and communication engineering. Then recorded temperatures are analyzed by an identification procedure. It allows the determination of  $H_p$  and  $H_e$  the transfer functions of the sample temperature variation due to heating power variation. The eigen-frequencies values of  $H_e$  and  $H_p$  are to equal  $\omega_{ext}$  and  $\omega_{int}$ .

#### 4. Results

Results corresponding to the flow reported on Fig. 4 are plotted on Fig. 5. They are the spectra of  $H_p$  the polar heat transfer function. The black curve is attached to the solid and acts as the reference. From those curves, the eigen-frequencies of transfer function are calculated and reported in Table 2. In order to compare with a value attached to the flow itself, we introduce  $\omega_{vortex}$  the turnover angular frequency of the vortices as well.

We see that the external angular frequency  $\omega_{ext}$  variation is less than 2%. Therefore, we are allow to affirm that the existence of the flow does not significantly modify the heat exchanges between the sample and the surrounding atmosphere (in the present case radiation only).  $\omega_{int}$  strongly evolves with the flow in a very similar way than  $\omega_{vortex}$ . Comparing those values leads us to affirm that higher  $Re_A$  is, more similar  $\omega_{int}$  and  $\omega_{vortex}$  are. The difference between those values is the highest for solid (i.e. vanishing velocity). Therefore, we may affirm that the heat transfer inside a molten sample is driven, for low velocity by both conduction and convection, and for high velocity by convection only. This result could appear to be straightforward, but it is not when considering the system approach chosen to analyze recorded temperature signals only.

Now, on Fig. 6, we plot the  $\omega_{int}$  values reported in Table 2 versus the  $|U|_{max}/U_A$  values deriving from the Fig. 4 graphs. These points are in line. The regression line crosses the y-axis in

**Table 2** Angular eigen-frequencies of the polar transfer function plotted on Fig. 5 compared with the turnover frequencies of the e.m. stirring vortex.

$v/v_o$	$Re_A$	$\omega_{vortex}$ ( $rd.s^{-1}$ )	$H_p$	
			$\omega_{ext}$	$\omega_{int}$
20	78.6	68.13	0.2112	65.80
40	39.3	35.70	0.2107	38.05
75	21.0	19.24	0.2101	22.87
100	15.7	14.72	0.2099	18.71
solid	0	0	0.2076	6.54

$B_{DC}$ (T)	$Ha$	$\omega_{vortex}$ ( $rd.s^{-1}$ )	$H_p$	
			$\omega_{ext}$	$\omega_{int}$
0.5	24	164.05	0.2113	162.90
0.6	28.7	124.05	0.2113	123.33
0.8	38.3	81.16	0.2113	79.53
1	47.9	57.58	0.2112	59.34
1.2	57.9	41.36	0.2110	48.34
solid	-	0	0.2076	6.54

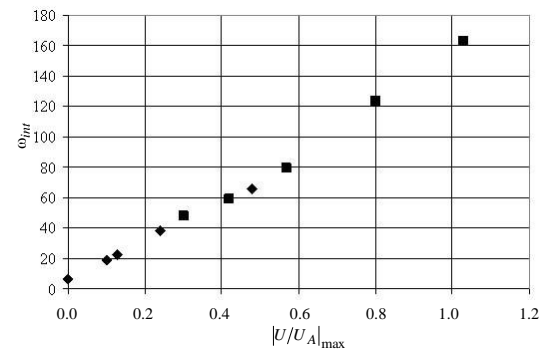


**Fig. 6** Internal angular eigen-frequency versus maximum velocity attached to Fig. 4 tiles : variation due to  $Re_A$  – squares : due to  $Ha$ .

the point corresponding to a vanishing velocity. Therefore, we may propose a new strategy for measuring both heat capacity and thermal conductivity of liquid metal alloy joining electromagnetic levitation plus a DC magnetic field and the here presented measurement protocol.

Measurements would be performed for two (or three) high enough magnetic field intensity values. The internal eigen-

frequencies would be calculated for each value and be plotted versus those values. Then the straight line connecting these points would be drawn. The point where this line crosses the y-axis is the eigen-frequency attached to the solid sample (i.e. thermal conductivity is controlling internal heat transfer) Then, on this eigen-frequency, simply apply a current calorimetry method as reported in <sup>3)</sup> or an inverse method to obtain both heat capacity or thermal conductivity.

## 5. Experimental validation

The experimental facility is sketched on **Fig. 7**. It is a standard levitation facility described in <sup>10)</sup>.

For the first trials, we chose a geometry as simple as possible: the sample is solid and as such that its thermophysical properties are known in the investigated temperature range. It is placed on a thermal insulating support and the inductor is similar to the inductor used in for space experiments and corresponds to **Fig. 3**. Power is modulated by a suitable white noise. Two dual band pyrometers are arranged on the axis and in the plane of the inductor. Signals collected by these pyrometers are treated according to the procedure described in <sup>7)</sup> implemented in a Matlab environment. In the examples below, the protocol is applied to a niobium bar (length : 100 mm and diameter : 10 mm).

**Figure 8** shows a result of the identification of the measured temperatures for the following experimental conditions: average inducting current: 211 A - amplitude of the modulation of the inducting current: 8% - base frequency of the inducting current: 94,195 Hz. The parameters for the LFSR are chosen as specified in annex 1 of reference (7) :  $N = 7$ ,  $k = 1$ ,  $t_s = 4s$  - total duration of the experiment: 500 s

On **Fig. 8**, we may see that the recorded signal are well recovered by the identification procedure. This procedure is applied for several inducting current intensities.

**Figure 9** is the representation of  $\tau_{ext} = 1/\omega_{ext}$  the evolution of the characteristic time of heat transfer between the sample and its environment versus the average surface temperature.

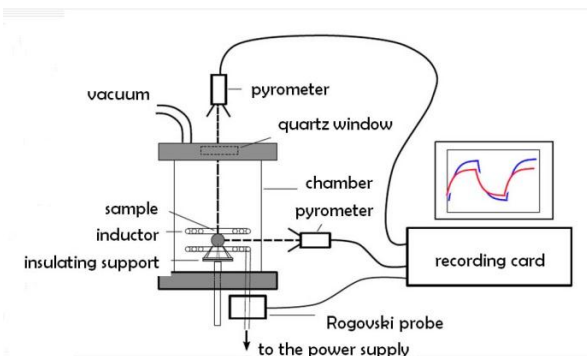


**Fig. 7** Experimental arrangement

We note that this time is intrinsic of the transfer functions  $H_p$  and  $H_e$ . It decreases with temperature. This trend is expected as the radiative transfers increase with the temperature of the surface of the sample.

The lower transfer time is  $\tau_{ext} = 132 s$ . By using the definition of this transfer time given by Fetch [2] i.e.  $C_p/4A\epsilon\sigma_B T_{moy}^3$  (where A and  $T_{moy}$  are respectively the area and the mean temperature at the surface of the bar, we found an emissivity  $\epsilon = 0.996$ . Taking into account that the used bar is oxidized, this value is a good order of magnitude of the emissivity.

**Figure 10** is the representation of the evolution of the heat capacity, calculated by Eq. (3) versus the mean temperature of the surface of the sample for both literature [11] and experimental values. There is a good agreement for the points corresponding to the highest investigated temperatures. The discrepancy attached to the lower temperature points could be due to the pyrometer accuracy. Indeed, the used pyrometers are not so precise in the range of temperature lying between 750 and 850 °C.

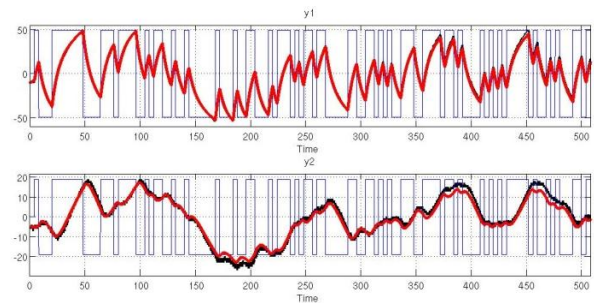


**Fig. 8** Identification of temperature variations generated by a white noise modulation of the Joule power (recorded blues curve-identified red curves) for above values - The upper and lower curves represent respectively the time-variation of equatorial temperature  $T_e$  and the polar temperature  $T_p$ .

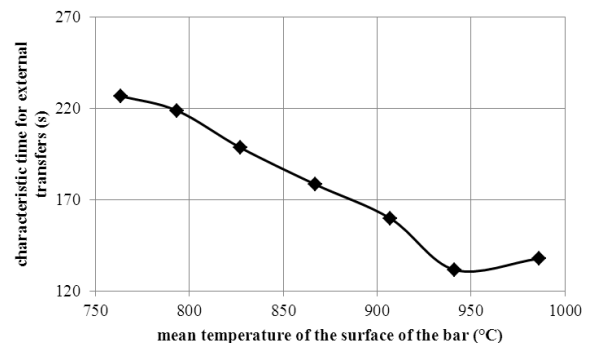


**Fig. 9** Evolution of  $\tau_{ext}$  the time characteristic of the heat transfers between the sample and its environment. This time is model free.

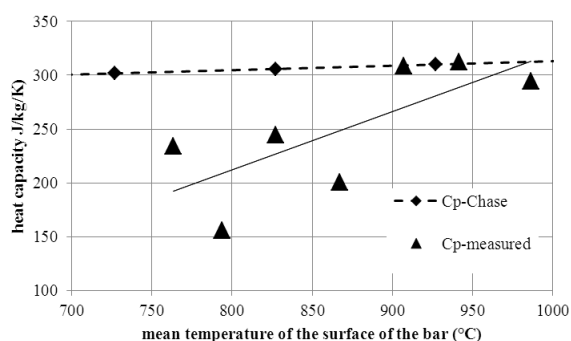


**Fig. 10** Evolution of the heat capacity versus the mean temperature of the surface of the sample. There is a good agreement for the points corresponding to the highest investigated temperatures.

## 6. Conclusion

In this article we presented some numerical experiments leading us to propose an original method of measurement derived from the traditional modulated calorimetry. It differs from existing methods on the following 3 points:

- use of electromagnetic levitation joined to a continuous magnetic field which intensity is high enough, as done by Kobatake <sup>12)</sup> but with different geometry,
- use of a temporal modulation of the Joule power dissipated into the sample in a white noise form,
- use of a signal analysis coming from process engineering to determine the eigen-frequencies attached to internal and external heat transfers.

This arrangement would allow the control of the flows in the levitated sample. The corresponding velocities could be slow enough in order the flow to be laminar. At two values of applied magnetic field are attached two values of eigen-frequency of the internal heat transfer. By interpolation of these two eigen-frequencies, we may find the frequency corresponding to the vanishing velocity. Knowing this point and using or an analytical method <sup>2)</sup> and <sup>3)</sup>, or an inverse method, we may

calculate the values of heat capacity and thermal conductivity of the sample.

A practical implementation of the procedure has been achieved on as simple as possible facility. Comparisons performed on measured and literature heat capacities are good enough to be sure that the used protocol is experimentally validated.

## Acknowledgement

This work has been funded by the followings supports : ESA under MAP-Thermolab, EC under PI-IMPRESS (Contract Number: NMP3-CT-2004-500635), CNES under Material Sciences Program. Author thanks Dr Mazen Al Amir (GipsaLab-Grenoble) for his invaluable help.

## References

- 1) I. Egry: *Mat. Trans.*, **45** (2004) 3235.
- 2) H. Fecht H and J. Johnson: *Rev. Sci. Instr.* **62** (1991) 1299.
- 3) R. Wunderlich and H. Fecht: *Measurement Science and Technology* **16** (2005) 402.
- 4) E.C Okress, D. M. Wroughton, G. Comenetz, P. H. Brace and J. C. R. Kelly: *Journal of Applied Physics* **23** (1952) 545.
- 5) I. Egry, A. Diefenbach, W. Dreier, and J. Piller: *International Journal of Thermophysics* **22** (2) (2001) 569
- 6) H.-J Fecht, A. Passerone, E. Ricci, J. Etay, I. Egry, S. Seetharaman: *Microgravity applications programme: Successful teaming of science and industry*. ESA SP-1290, ESTEC, Noordwijk, Netherlands: ESA Publications Division, (2005) 8
- 7) P. Schetelat and J. Etay: *Heat and Mass Transfer* **47** (7) (2011) 759
- 8) V. Bojarevics, S. Easter, A. Roy and K. Pericleous: *Proceedings of the International Symposium on Liquid Metal Processing and Casting - LMPC 2009*. The Minerals, Metals & Materials Society, Warrendale, Pennsylvania, USA (2009) 319
- 9) Y. Delannoy, J. Etay and Y. Fautrelle: *Proceedings of the International PAMIR conference, Ramatuelle (France)*, (2002) section II 39-44
- 10) J. Etay, Y. Fautrelle, A. Gagnoud, Y. Duterrail, D. Perrier & B. Bardet : *Mécanique et Industrie*- **5** (2004) 627
- 11) M. Chase : *Journal of Physical and Chemical Reference Data*, **9** (1998) 959-1951
- 12) H. Kobatake, H. Fukuyama, I. Minato, T. Tsukada and S. Awaji: *Appl. Phys. Lett.* **90**, (2007) 094102.

(Received 9 Oct. 2012; Accepted 25 Dec. 2012)